Tilt Angle of Bipolar Active Regions from Solar Cycle 23

Mariano Poisson[1] iD

Abstract
Active regions (ARs) are the photospheric manifestation of the emergence of magnetic flux ropes (FRs) formed in the solar interior. A key parameter in an AR evolution is its tilt angle, defined as the inclination of the AR polarity axis with respect to the solar equator, which plays a central role in flux-transport dynamo models that explain the cyclic transformation of toroidal to poloidal magnetic fields. However, measuring the tilt angle is affected by projection effects, such as magnetic tongues, particularly during the AR emergence phase. In this work, we analyze tilt angle estimations for 126 bipolar ARs from Solar Cycle 23 using two methodologies: (1) the conventional magnetic barycenter method, which calculates the bipole axis based on the centroids of the polarities, and (2) a Bayesian FR method, which employs synthetic magnetograms simulating the emergence of a twisted toroidal flux tube to fit observed AR magnetograms via Bayesian inference. The Bayesian FR method accounts for projection effects and provides a more accurate estimation of the intrinsic tilt, especially during the early stages of emergence when magnetic tongues are most extended. We perform a statistical analysis of tilt angle evolution, showing that the Bayesian FR method reduces tilt dispersion providing a more reliable estimation of Joy's law.

Keywords: Active Regions, Magnetic Fields; Active Regions, Models;Magnetic fields, Photosphere

1. Introduction

Active regions (ARs) are fundamental manifestations of the Sun's magnetic activity and play a crucial role in shaping the dynamics of the solar cycle. Their evolution is directly linked to solar eruptions, coronal mass ejections, and

M. Poisson
mpoisson@iafe.uba.ar

[1]   Instituto de Astronomía y Física del Espacio, CONICET-UBA,CABA, Argentina.

space weather phenomena (Schrijver and Zwaan 2000; Toriumi and Wang 2019). Understanding the formation and magnetic properties of ARs has been a long-standing focus in solar physics, driving advances in observational techniques and theoretical modeling.

A key mechanism underlying AR formation is the emergence of magnetic flux ropes (FRs)—twisted bundles of magnetic field lines formed in the solar interior. These structures rise buoyantly through the convection zone due to a combination of magnetic pressure and reduced plasma density (Fan 2001; Cheung and Isobe 2014). The degree of twist in an FR influences its stability and likelihood of producing solar eruptions, with highly twisted FRs being more prone to destabilization (Liu et al. 2016; Török et al. 2018).

In line-of-sight magnetograms, FR twist manifests as elongated polarity extensions known as magnetic tongues.. These features, which arise due to the azimuthal component of the FR magnetic field, are most prominent during the early stages of AR emergence (Luoni et al. 2011; Poisson et al. 2016). Their presence alters the observed magnetic flux distribution, affecting the determination of key AR properties, including the tilt angle.

The tilt angle of an AR—defined as the angle between the line connecting the centroids of opposite polarity regions and the solar equator—is a critical parameter in dynamo models, as it plays a fundamental role in regulating the solar magnetic cycle (Stenflo and Kosovichev 2012). The statistical tendency for the tilt angle to increase with latitude, known as Joy's law, serves as a key input for flux-transport models that simulate large-scale solar magnetic field evolution (Hale et al. 1919; Dasi-Espuig et al. 2010; Yeates et al. 2023).

Determining the tilt angle with precision is challenging due to the complexity of AR emergence. Magnetic tongues, in particular, shift the apparent positions of polarity centroids, introducing systematic biases in tilt angle measurements (Poisson et al. 2022). Correcting for these distortions is essential to refine tilt angle estimates and to investigate deviations from Joy's law, such as the observed suppression of tilt at high flux values (Jiang 2020).

In Poisson et al. (2016), a statistical study of bipolar ARs from Solar Cycle 23 demonstrated that magnetic tongues serve as a proxy for FR twist and significantly impact tilt angle measurements. The study highlighted the necessity of correcting for these effects, especially when discrepancies arise between different tilt estimation methods.

Building on this, Poisson et al. (2020a) introduced the Core Field Fit Estimator (CoFFe), a method designed to estimate the intrinsic inclination of FRs. This technique effectively mitigates the impact of magnetic tongues, leading to more reliable tilt angle measurements. A subsequent comparison between CoFFe and other methods, such as those based on flux-weighted polarity centroids and white-light observations, revealed substantial differences in derived tilt angles (Poisson et al. 2020b).

Expanding upon these efforts, Poisson et al. (2022) applied Bayesian inference to model FR emergence using line-of-sight magnetograms. This approach, which approximates the FR as a half-torus, was validated against synthetic data and a single observed AR, demonstrating improved robustness in recovering key FR

parameters. However, the method was limited to single-magnetogram analyses, leaving room for further refinement.

In Poisson et al. (2024), the Bayesian method was extended to incorporate temporal coherence, allowing inferred parameters to evolve smoothly over time. This refinement provided a dynamic representation of the emergence process and enabled a more detailed exploration of parameter constraints. The study identified optimal prior selections and parameter space configurations, advancing our understanding of FR evolution.

In this article, we extend previous analyses by applying Bayesian inference to a large dataset of 126 bipolar ARs from Solar Cycle 23. Our objectives are threefold: (1) refine tilt angle corrections, particularly during early emergence stages, addressing biases introduced by magnetic tongues. (2) Evaluate the impact of these corrections on Joy's law and assess their implications for solar dynamo models. (3) Compare Bayesian-inferred tilt angles with traditional methods, such as those based on magnetic barycenters, and analyze discrepancies. Section 2 introduces the dataset, Section 3 summarizes the Bayesian method, Section 4 compares tilt estimates from both methods, and Section 6 summarizes our findings and their implications for solar cycle modeling.

2. AR selection and Data Processing

We analyzed the evolution of 126 bipolar ARs using line-of-sight (LOS) magnetograms from the Michelson Doppler Imager (MDI; Scherrer et al. 1995) onboard the Solar and Heliospheric Observatory (SOHO). This dataset spans almost the full duration of Solar Cycle 23 (July 1996–January 2010). MDI produced full-disk magnetograms at a 96-minute cadence by averaging either one-minute or five-minute magnetograms, with flux density errors of 16 G and 9 G per pixel, respectively (Liu, Zhao, and Hoeksema 2004). Each day, 15 magnetograms were available, with a resolution of 1024×1024 pixels and a spatial scale of $1.98''$ per pixel.

Figure 1 displays the latitude and emergence time of the 126 bipolar ARs from our selected dataset. The ARs were selected based on three main criteria. (1) Bipolar configuration: ARs had to predominantly maintain a simple β structure. (2) Emergence coverage: data had to span from initial flux detection to a few hours after maximum flux. (3) Projection effects: ARs were restricted to $|\text{latitude}| \leq 35°$ and $|\text{longitude}| \leq 60°$. The top and left histograms in Figure 1 indicate that the majority of the ARs in our sample corresponds to the period around Solar Cycle 23 maximum, with most ARs located within latitudinal bands of approximately $10°$ to $30°$ in both hemispheres.

To analyze the temporal evolution of each AR, we constructed data cubes encapsulating their photospheric magnetic field. First, LOS magnetograms were converted to the radial field under the assumption of radiality. Second, all magnetograms were derotated to align with the frame closest to the central meridian passage. Third, AR subfields were extracted from the full-disk maps to enclose the complete magnetic structure. Finally, we extract the subregions from the full-disk magnetograms that fully enclose each AR's magnetic structure. For
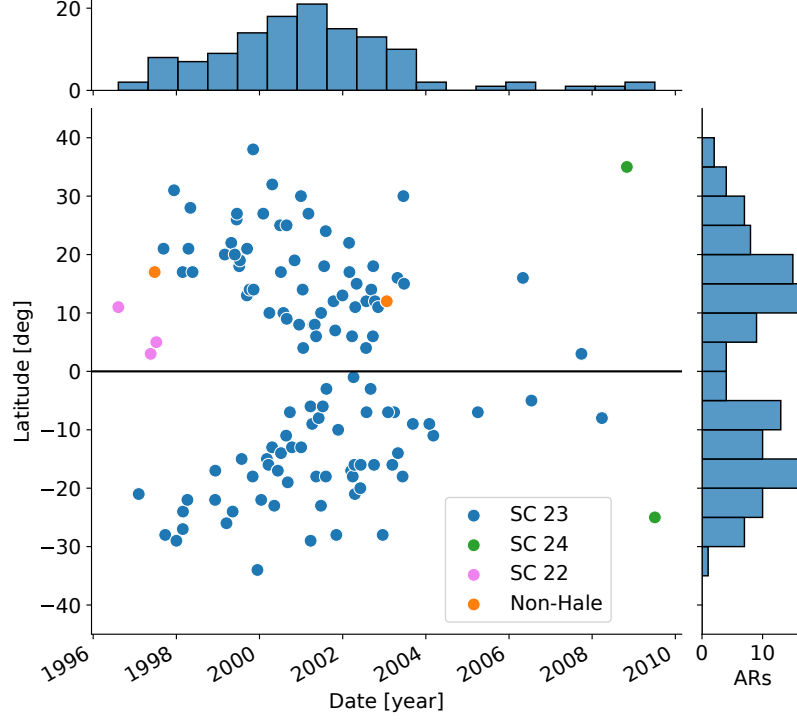
Figure 1. Butterfly diagram of the 126 bipolar ARs in our sample. Blue dots correspond to ARs emerging in Solar Cycle 23. Violet and green dots correspond to ARs from Cycles 22 and 24, respectively, while orange dots mark the non-Hale bipoles. The top histogram shows the temporal distribution of AR emergences (bin size 6 months), and the right histogram shows their latitudinal distribution (bin size 5°).

further details on the data processing pipeline, we refer to Poisson et al. (2022, 2024).

To enable a temporal comparison across different ARs, we define a normalized time axis (t_{norm}), where $t_{norm} = 1$ corresponds to the time of maximum observed magnetic flux. The origin, $t_{norm} = 0$, is defined as the extrapolated time when the AR net flux reaches zero. This extrapolation is obtained by performing a linear fit to the flux evolution over the first quarter of the interval bounded by the initial observed magnetogram and the magnetogram corresponding to maximum flux. In this way, t_{norm} provides a common reference frame to compare different stages of AR emergence, independent of the actual duration of the emergence in each individual case.

To ensure a homogeneous and consistent dataset, we excluded ARs for which either the initial or final phase of the emergence could not be fully tracked due to the longitudinal restrictions imposed in the selection criteria. After this filtering, our final sample consists of 108 ARs.
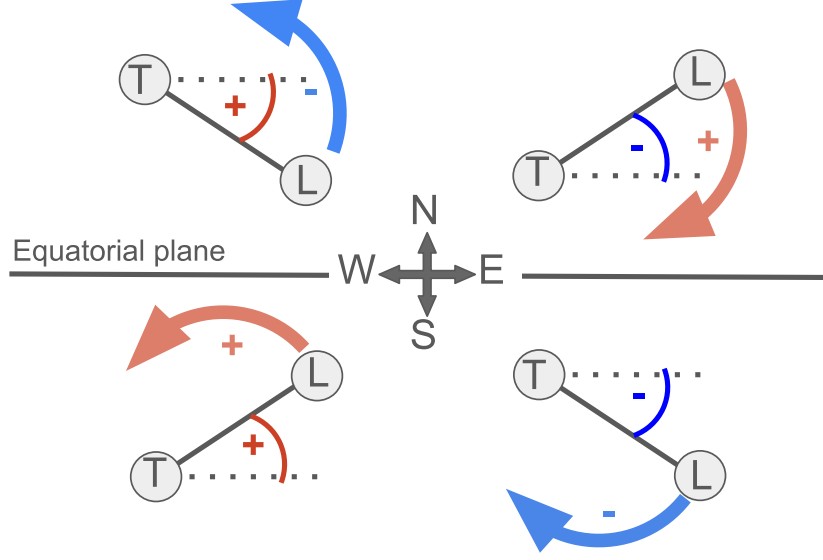
Figure 2. Diagram illustrating the sign convention used for the tilt angle (α) and the bipole rotation (γ). The horizontal line represents the solar equator, with "T" and "L" denoting the trailing and leading polarities, respectively. Positive (negative) α is shown in red (blue) and corresponds to cases where the leading (trailing) polarity is closer to the equator. Positive rotation represents a shift where the leading polarity moves toward the equator, whereas negative rotation occurs when the leading polarity shifts away from the equator.

3. Estimation of the Tilt Angle of ARs

In general, estimating the tilt angle relies on accurately identifying the polarities of an AR. Historically, white-light images were used, where the umbra and penumbra areas of sunspots helped to pinpoint the strong flux contributions of each polarity, allowing for the identification of the centers of the leading and trailing polarities. The tilt angle was then defined by the inclination of the line connecting these two centers relative to the equatorial plane (see, e.g., Baranyi, Győri, and Ludmány 2016).

However, a challenge arises when diffuse or weak magnetic flux regions, particularly in trailing polarities, fail to form clear sunspots. This issue has been resolved with the use of LOS magnetograms, which allow for clear identification of positive and negative polarities. For simple bipolar ARs, it becomes straightforward to calculate the flux-weighted centers (barycenters) of the leading and trailing polarities, enabling more precise tilt angle estimation (e.g., López Fuentes et al. 2000). We will refer to this estimation of the tilt as simply α_{bar}. In previous studies, we compared tilt angle estimates obtained from LOS magnetograms of specific bipolar ARs with those derived from white-light images (Poisson et al. 2022). Although both methods produced generally consistent results, we found that magnetic tongues significantly influence the evolution of the estimated tilt during the early phases of an AR development.

Figure 2 shows a diagram defining the sign convention used in this work for both the tilt angle (α) and bipole rotation (γ), independently of the method used

to estimate these quantities. The tilt angle is measured within a range of $-90°$ to $90°$. This range could pose a problem for ARs exhibiting significant rotations, as seen in some δ-type sunspots. However, in our dataset of bipolar ARs, we do not find cases in which the rotation results in an East-West reversal of leading and trailing polarities. In our convention, a positive/negative tilt is assigned when the leading polarity is closer/farther to the equator in either hemisphere. γ reflects how the tilt evolves during a given interval of time that we set to one day. We define a positive/negative rotation when the leading polarity shifts toward/away the solar equator. The bipole rotation angle γ tracks the changes in the AR tilt as its magnetic field evolves. A positive/negative γ brings the leading polarity closer/farther from the equator. These sign conventions allow for a direct comparison of tilt behavior across hemispheres.

The Bayesian method provides a novel measure of the emerging FR tilt. This method describes the emergence of ARs using a magnetic FR model with a half-torus geometry, in which the twist is quantified by the number of field-line turns around the torus axis (see Poisson et al. 2022, 2024). This framework provides a simplified, large-scale description of the line-of-sight (LOS) magnetic field in bipolar ARs. While it does not include small-scale distortions due to reconnection or plasma flows during the complex emergence process, it captures the dominant magnetic structure and its temporal evolution.

To constrain the FR parameters, we generate synthetic magnetograms by computing the vertical field component onto cross-sections of the torus at different heights and comparing them with observations within a statistical Bayesian framework. The model includes four parameters describing the FR itself—minor radius (a), major radius (R), axial magnetic flux (Φ_A), and twist (N_t)—and four positional parameters—(x_c, y_c), depth d_0, and tilt α. Following Poisson et al. (2024), we apply the model to time-series magnetograms, assuming that field parameters remain constant during emergence except for a, which evolves to account for expansion, while positional parameters vary with time. This temporal formulation improves parameter stability and ensures a coherent description of the emergence process (see also Poisson et al. 2025).

The presence of magnetic twist introduces at the photospheric level elongated magnetic polarities, or magnetic tongues, which evolve during the emergence. Then, the amount of twist biases the tilt estimation of the magnetic barycenter method. In contrast, using a magnetic FR model accounts for the influence of magnetic tongues, removing their effect on the tilt, then providing an estimate that aligns closer with the intrinsic inclination of the emerging FR. We will refer to this estimation of the tilt as α_{mod}, indicating it is obtained from modeling the AR photospheric flux distribution.

4. Comparing Tilt Angle Estimation Methods

4.1. AR 9290

Figure 3 illustrates the application of our method to AR 9290. The left panels display LOS magnetograms at representative stages of emergence while the right
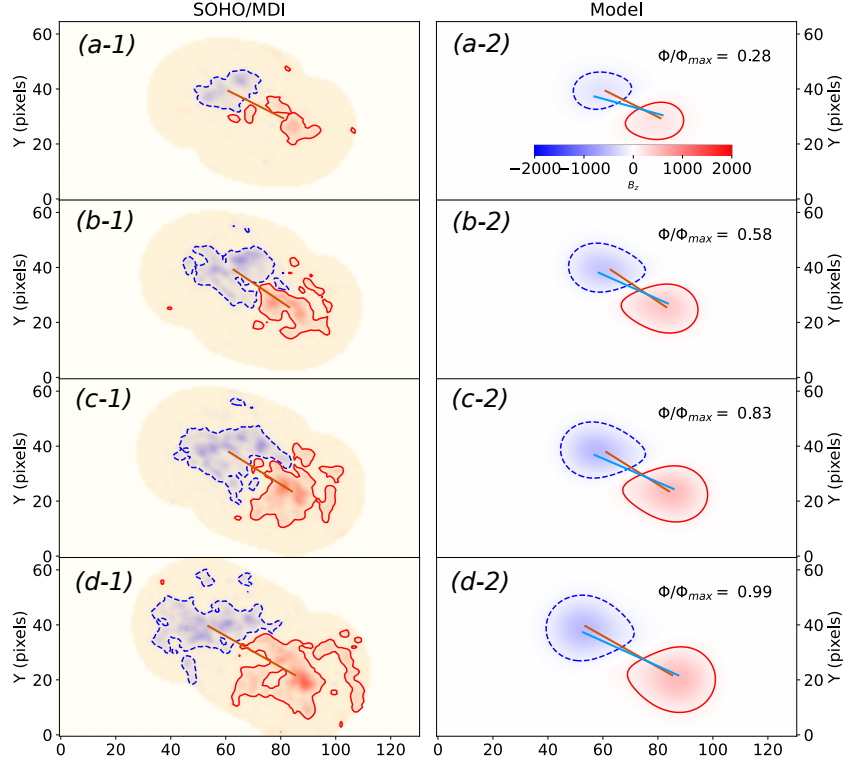
Figure 3. Observed LOS magnetograms (left) and corresponding most probable FR models (right) at four stages of the emergence of AR 9290. Blue and red shading denote negative and positive LOS magnetic flux density, respectively. Solid red and dashed blue contours mark the ±100 G levels. Orange segments connect the flux-weighted centroids of the polarities, with their orientation relative to the x-axis indicating the tilt derived from the magnetic barycenter method. In contrast, pale blue segments connect the modeled FR axis footpoints and provide an alternative tilt estimate obtained through the Bayesian approach.

panels show the corresponding most probable FR models. The fitting masks are outlined in yellow in the left panels (see Poisson et al. 2025). The corresponding normalized magnetic flux (to the maximum flux) are indicated in the right panels. During the early phases of emergence at latitude ∼N30°, the magnetic polarities appear elongated, forming magnetic tongues consistent with a negatively twisted FR. These tongues displace the flux-weighted centroids toward the polarity inversion line, leading to an apparent inclination of the bipole as measured by the barycenter method (black segments). In contrast, the modeled FR axis footpoints (green segments) provide an alternative tilt estimate that is more robust against the influence of magnetic tongues.

The temporal evolution of the tilt angle is shown in Figure 4a for both the Bayesian approach (α_{mod}, blue) and the barycenter method (α_{bar}, orange). Shaded areas indicate the 1σ uncertainties associated with each estimate. For α_{bar}, uncertainties were derived by averaging results obtained using four different field-strength thresholds, corresponding to all pixels, those above the median of the field-strength distribution, twice, and three times this median as a threshold
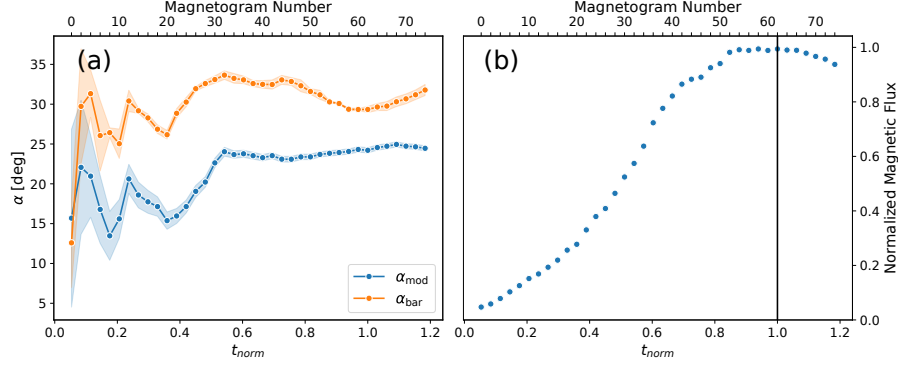
Figure 4. (a) Evolution of the tilt angle, α, of AR 9290 estimated using the Bayesian (α_{mod}) and the barycenters methods (α_{bar}) with blue and orange dots, respectively. The shaded area represents the error of each estimate, as indicated by its standard deviation. (b) Evolution of the normalized magnetic flux of AR 9290. This curve is used as a reference to determine the values of 0 and 1 for the normalized time.

for the field. For α_{mod}, the mean and standard deviation were computed from the sampled marginal posterior distribution. The time axis is normalized such that $t_{\mathrm{norm}} = 1$ corresponds to the maximum net flux of the AR, whose evolution is shown in Figure 4b.

Both methods yield broadly consistent tilt evolution for AR 9290, though with a systematic offset of 5°–10° across most of the emergence. The Bayesian estimate α_{mod} indicates a consistently smaller inclination than α_{bar}, with the maximum discrepancy occurring during the first half of emergence, when the effect of the tongues is more important. The gap narrows toward the later stages, yet does not vanish entirely, suggesting that factors beyond projection effects—such as the influence of magnetic tongues or intrinsic model assumptions—contribute to the residual differences between the two methods.

4.2. General Comparison

In this section we compute the evolution of tilt angles for the full sample of 108 ARs using both the Bayesian FR method (α_{mod}) and the barycenter method (α_{bar}). Figure 5a shows the normalized magnetic flux evolution for all ARs as a function of the normalized time t_{norm}. Each dot corresponds to an estimate from a single magnetogram, while larger dots and shaded areas indicate the mean and standard deviation within different bins of t_{norm}. The flux evolution curves exhibit a consistent pattern across the sample, with a rapid initial increase followed by a gradual approach to maximum flux. The dispersion in flux values is more pronounced during the early emergence stages, reflecting the variability in AR growth rates. This curve show a good correlation between the growth of t_{norm} and the AR magnetic flux suporting its use as a temporal reference for the emergence process. The histogram in Figure 5b displays the distribution of maximum magnetic flux values for the 108 ARs. The distribution is right-skewed, with a median value of 8.2×10^{21} Mx, indicated by the red dashed vertical line.
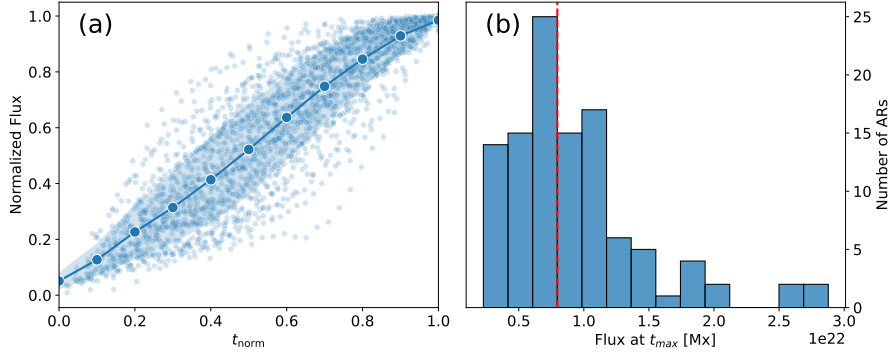
Figure 5. (a) Magnetic flux normalized to the maximum flux for 108 ARs as a function of the normalized time t_{norm}. Each dot corresponds to estimates over a single magnetogram. Larger dots and shaded areas indicate the mean and standard deviation within different bins of t_{norm}. (b) Histogram of the maximum magnetic flux of the ARs. Red-dashed vertical line indicates the median of the distribution showing the samples used to group low and high flux ARs

This median value is used to categorize ARs into low-flux and high-flux groups for further analysis.

We assess the correlation between the two tilt estimates for the 108 ARs by comparing α_{mod} with α_{bar} (Figure 6a). Each point corresponds to the mean tilt value of a given AR within one of eleven bins defined along the normalized time axis ($0 \leq t_{norm} \leq 1$). This procedure yields a total of 1111 points, fewer than the 1188 possible, since some ARs lack measurements close to the first bin near $t_{norm} = 0$. A linear least-squares fit to the scatter plot gives a slope of 0.57 and a Pearson correlation coefficient of 0.63, indicating a moderate correlation between the two methods. On average, the Bayesian estimates yield systematically smaller tilt angles than the barycenter method. High-flux and low-flux ARs, represented by orange and green lines respectively, exhibit similar trends, with slopes of 0.50 and 0.64 and correlation coefficients of 0.61 and 0.66, respectively. This consistency suggests that the systematic differences between the two methods are not strongly dependent on the AR magnetic flux.

The comparison of tilt signs further reveals that $\sim 63\%$ of the values correspond to positive tilts for both methods, i.e., with the leading polarity closer to the equator. In contrast, $\sim 22\%$ of the cases show negative tilts in both estimates. Discrepancies of tilt sign between the two approaches arise in the remaining fraction of cases: about 10% are positive in α_{mod} but negative in α_{bar}, while $\sim 6\%$ show the opposite behavior. These differences highlight the sensitivity of the tilt sign determination to the method employed, particularly in bipoles which are closely oriented towards the EW direction.

Figure 6b shows the histograms of the mean tilt values per AR per bin along t_{norm}. The two methods yield very similar distributions, both in terms of mean values and dispersion, with α_{mod} shown in blue and α_{bar} in orange. This indicates that, despite the systematic differences seen in the direct comparison, both estimations capture a consistent range of tilt angles within our sample of ARs.
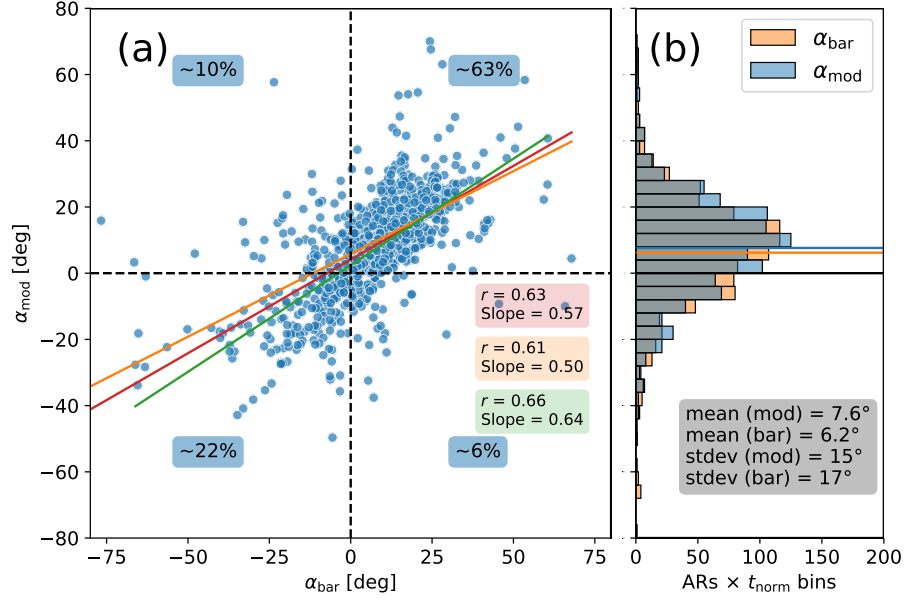
Figure 6. (a) Comparison of tilt angles estimated with the Bayesian FR method (α_{mod}) and the barycenter method (α_{bar}) for 108 ARs. Each point represents the mean tilt within a t_{norm} bin. The red, orange, and green lines show the linear least-squares fit of the full sample, the high-flux sample, and the low-flux sample, respectively. (b) Histogram of tilt angle distributions for both methods, with α_{mod} in blue and α_{bar} in orange.
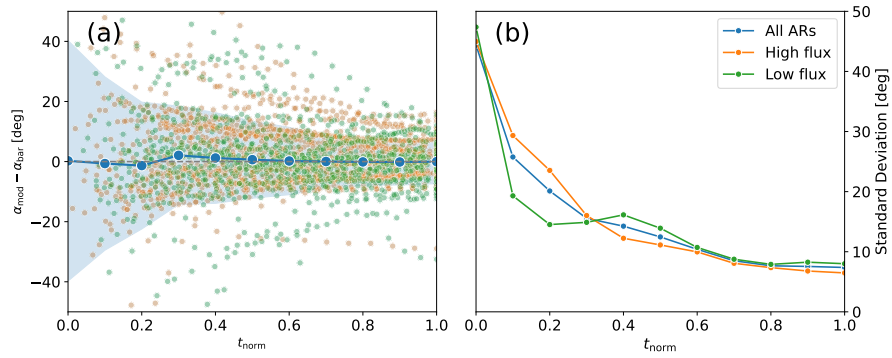

Figure 7. (a) Evolution of the difference between Bayesian FR and barycenter tilt estimates ($\alpha_{\mathrm{mod}} - \alpha_{\mathrm{bar}}$) for all analyzed magnetograms of 108 ARs. Blue dots indicate the median value within each t_{norm} bin, and the shaded area represents the 1-σ standard deviation. Green and orange dots corresponds to the difference for ARs with lower and higher flux respectively. (b) Evolution of the 1-σ standard deviation of the difference between tilt estimations for the same groups.

We compute the difference between the two methods as $\alpha_{\mathrm{mod}} - \alpha_{\mathrm{bar}}$ and analyze how it evolves during the emergence of 108 ARs. Figure 7a shows this difference as a function of t_{norm}, which provides a common temporal reference for the different ARs. Solid blue dots with connecting lines correspond to the median values at each temporal bin, and the shaded areas indicate the corresponding standard deviation. The green and orange dots represent the differences for low-flux and high-flux ARs, respectively. Across the entire sample, the median difference remains close to zero throughout the emergence process, indicating no significant systematic bias between the two methods on average. However, the standard deviation of the differences, shown in Figure 7b, reveals a clear trend: it decreases from approximately 40° at $t_{\mathrm{norm}} = 0$ to about 8° at $t_{\mathrm{norm}} = 1$. This indicates that the two methods converge toward similar tilt estimates as the ARs approach their maximum flux.

The largest difference between α_{mod} and α_{bar} during the early stages of emergence is expected due to the influence of magnetic tongues, which decrease as the tongues retract toward the end of emergence. The distribution of differences becomes close to normal for $t_{\mathrm{norm}} \geq 0.5$, symmetrically distributed around a mean of zero. These distributions with decreasing standard deviations suggest that our sample includes a wide variety of effects that bias the barycenter-based estimation of the tilt. In particular, the normal distribution indicates that the emerging FRs likely span a broad range of twist values, producing tongues of different strengths and, consequently, varying projection effects on α_{bar}.

Figure 8a shows the temporal evolution of the tilt angle, α, as a function of t_{norm} for the full sample of 108 ARs. The blue and orange curves correspond to values derived from the tilt angles obtained with the model (α_{mod}) and with the magnetic barycenters (α_{bar}), respectively. Both methods reveal a broadly similar trend despite case by case differences presented in Figure 7. Median values represented by solid dots connected with lines mantain stable between $\sim 6°$ and $\sim 10°$ throughout the emergence process. The broad dispersion of points reflects the large variability in the tilt angles across different ARs, including different fluxes and latitudes of emergence.

Figure 8b and c display the evolution of α for the low-flux and high-flux sub-samples, respectively. For both estimation methods the high-flux ARs present systematically larger tilt angles than the low-flux ARs, an effect that is most noticeable during the early stages of emergence. The shift in the median tilt between the two groups is driven largely by a reduction in the number of negative-tilt cases in the high-flux sample (fewer occurrences where the leading polarity is displaced away from the equator). This finding suggests that stronger, high-flux regions are less prone to the tongue-induced or convective biases that inflate the occurrence of negative tilts at low flux. This effect is more clearly captured by the Bayesian estimate α_{mod}, which yields a cleaner signal with reduced scatter.

We compute the rotation rate of the bipole γ as a function of t_{norm} in Figure 8d. We separated ARs with a positive (solid lines) and negative (dashed lines) total accumulated rotation. Blue dots and orange triangles indicate the median of γ within temporal bins. Both estimates present similar trends in which rotations are stronger at early phases of the emergence and tilts tend to stabilize by the time of the maximum flux. Panels (e) and (f) show same trend for γ for
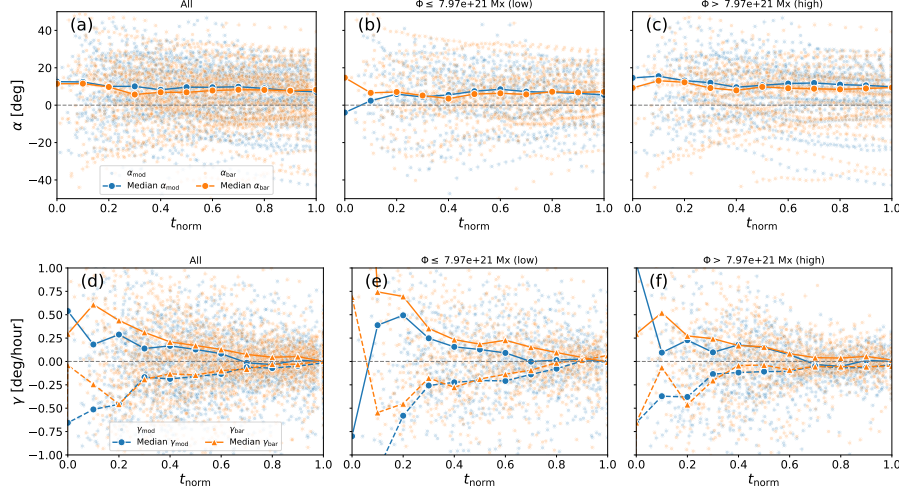
Figure 8. Top row: Evolution of the tilt angle for 108 ARs. Dots indicate the estimation of α obtained with the Bayesian method (blue) and the barycenter method (orange). Solid dots indicate the median value within each t_{norm} bin for each estimate. We group the sample using all 108 ARs (a), those with low magnetic flux (b), and those with higher flux (c). Bottom row: Evolution of the angular rotation rate γ for all 108 ARs (d), low flux (e), and high flux ARs (f). Solid (dashed) lines join median values within t_{norm} bins for ARs in which total accumylated rotation is positive (negative).
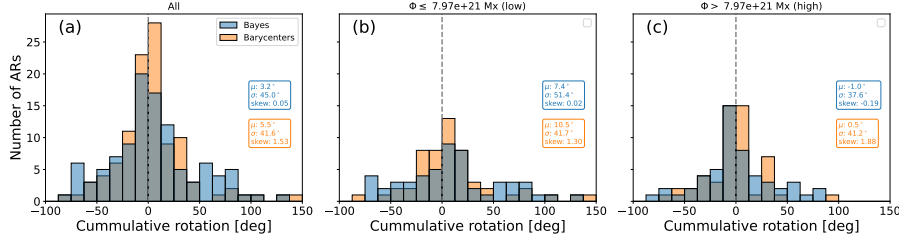

Figure 9. Distribution of the cumulative rotation during AR emergence. Blue and orange histograms show cumulative rotations obtained with the Bayesian method and the barycenter method, respectively. Panels correspond to (a) the full sample of 108 ARs, (b) the low–flux subsample, and (c) the high–flux subsample.

the low-flux and high-flux sub-samples. Comparing these samples we find that low-flux ARs presents stronger mean rotations along the emergence by a factor 2 than the high-flux ARs.

The larger dispersion of γ_{bar} during early emergence (compared to γ_{mod}) indicates that barycenter-based rotation estimates are more affected by transient effects such as magnetic tongues and small-scale flux rearrangements, while the Bayesian FR estimate provides a cleaner, more stable measure of the intrinsic bipole rotation. The decreasing trend observe for both estimates is more likely associated to the emergence process in which convective buffeting over the FR is less effective as the AR flux increases and polarities apart from each other.
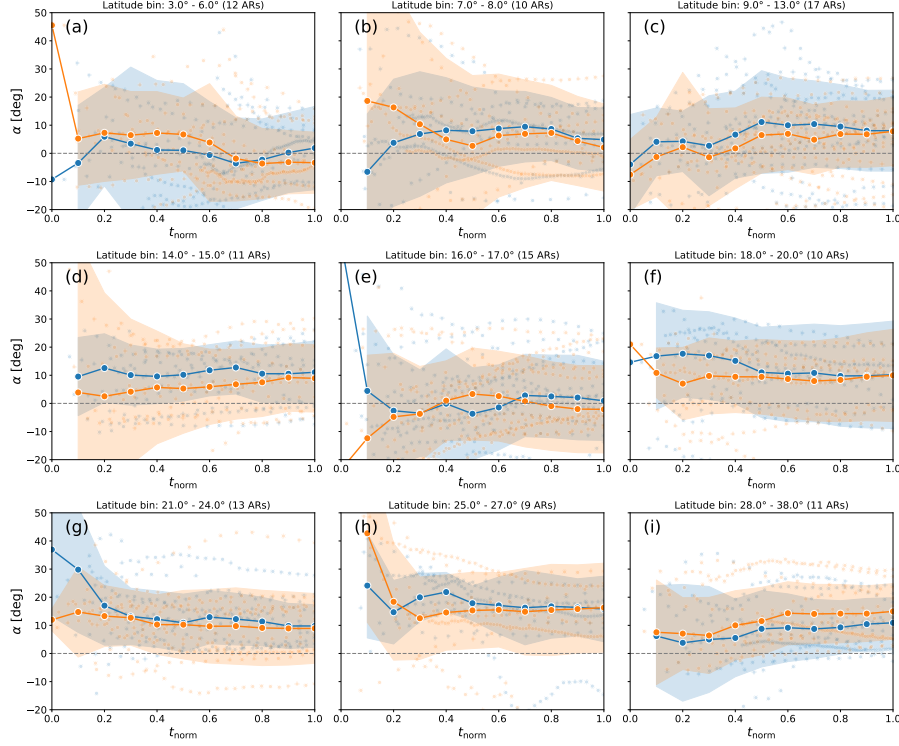
Figure 10. Evolution of α as a function of the normalized time t_{norm} for different latitudinal bins. Each panel corresponds to a specific latitude bin, with solid lines representing the median α values and shaded areas indicating the standard deviation. Scatter points show individual data points.

Figure 9 shows the distribution of the total accumulated rotation, computed as $\sum_{t=0}^{1} \gamma \, \Delta t$, for (a) the full sample of 108 ARs, (b) the low–flux subsample, and (c) the high–flux subsample. In each panel blue and orange histograms correspond to the Bayesian and barycenter estimates, respectively. Both methods yield similar central values and overall dispersions, indicating comparable rotation magnitudes on average. However, the Bayesian-derived distributions are generally more symmetric and closer to a normal shape, while the barycenter-derived distributions display larger skewness. This reduced asymmetry suggests the Bayesian method produces more robust cumulative-rotation estimates by mitigating biases from magnetic tongues and short-term flux rearrangements; the near-symmetric Bayesian distributions are consistent with convective buffeting acting predominantly as a stochastic driver of bipole rotation. [Mariano comment: Still effect is small over few cases and both methods suggest that convective buffeting is the main contribution to AR rotations.]
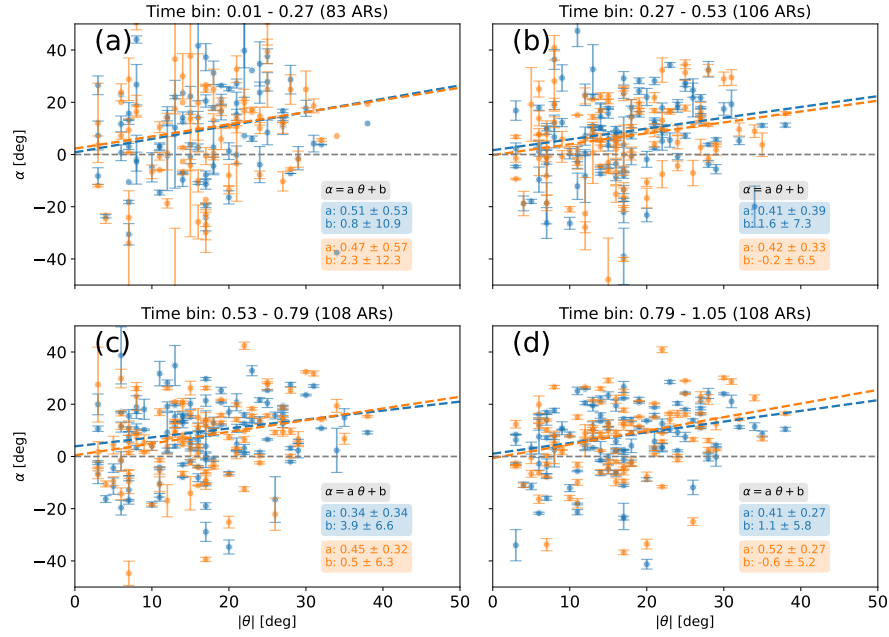
Figure 11. Mean tilt as a function of latitude for different normalized time bins. Each panel corresponds to a specific normalized time bin, with blue (orange) dots representing α_{mod} (α_{bar}) individual data points. The dashed lines indicate the linear least-squares fits for both methods.
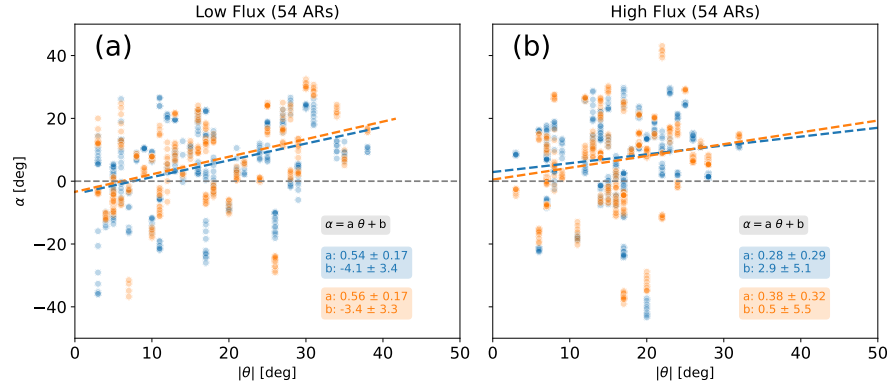

Figure 12. Mean tilt as a function of latitude for low (a) and high (b) flux ARs. On each panel the blue (orange) dots represents α_{mod} (α_{bar}) individual data points. The dashed lines indicate the linear least-squares fits for both methods.

Table 1. RMS error and Pearson correlation (rho) by time bin.

Time bin	RSME α (deg)	ρ_α	RSME α_{bar} (deg)	$\rho_{\alpha_{\text{bar}}}$
-0.10 − 0.40	17.67	0.1397	18.97	0.1926
0.40 − 0.62	14.93	0.1598	14.75	0.2621
0.62 − 0.83	13.05	0.2206	13.84	0.2656
0.83 − 1.05	12.72	0.2742	13.10	0.2971

Table 2. RMS error and Pearson correlation by flux group.

Group	RMSE α (deg)	ρ_α	RMSE α_{bar} (deg)	$\rho_{\alpha_{\text{bar}}}$
Low Flux	11.68	0.391216	11.55	0.409670
High Flux	13.48	0.131941	14.59	0.161803

5. Latitudinal dependance of the Tilt Angle

5.1. Filtering effect of turbulent buffeting

[Mariano comment: Reducing outliers assuming a latitudinal dependence $\propto \sin(\theta)$]

5.2. Comparing Joy's Law

[Mariano comment: Comparative for different moments of the AR emergence]

5.3. Tilt Quenching?

[Mariano comment: Tilt dependence of the Flux Strength?]

6. Summary and Conclusions

P comment: The following limitations can be kept for the conclusion, calling for an extension of the model. Here it is too much lowering the usefulness of the method: Still, present model does not account for other effects, such as an asymmetry of polarities in directions parallel/orthogonal to the AR axis, or magnetic tongues with different extensions in both polarities. Such asymmetries can still introduce discrepancies between the inferred and true tilt.

P comment: This is more for a discussion section: The model, however, has its own limitations when estimating the field distribution at early times, since it assumes symmetric circular cross-sections. In contrast, the initial stages of emergence are often characterized by fragmentation of the main FR, followed by reformation through magnetic reconnection. Nevertheless, the average behavior of α_{mod} during these stages is expected to be less affected by observational biases than α_{bar}. P comment: because remove tongue effects?

Declarations

References

Baranyi, T., Győri, L., Ludmány, A.: 2016, On-line Tools for Solar Data Compiled at the Debrecen Observatory and Their Extensions with the Greenwich Sunspot Data. *Sol. Phys.* **291**, 3081. DOI. ADS.

Cheung, M.C.M., Isobe, H.: 2014, Flux Emergence (Theory). *Living Reviews in Solar Physics* **11**, 3. DOI. ADS.

Dasi-Espuig, M., Solanki, S.K., Krivova, N.A., Cameron, R., Peñuela, T.: 2010, Sunspot group tilt angles and the strength of the solar cycle. *Astron. Astrophys.* **518**, A7. DOI. ADS.

Fan, Y.: 2001, The Emergence of a Twisted Ω-Tube into the Solar Atmosphere. *Astrophys. J. Lett.* **554**, L111. DOI. ADS.

Hale, G.E., Ellerman, F., Nicholson, S.B., Joy, A.H.: 1919, The Magnetic Polarity of Sun-Spots. *Astrophys. J.* **49**, 153. DOI. ADS.

Jiang, J.: 2020, Nonlinear Mechanisms that Regulate the Solar Cycle Amplitude. *Astrophys. J.* **900**, 19. DOI. ADS.

Liu, J., Wang, Y., Erdélyi, R., Liu, R., McIntosh, S.W., Gou, T., Chen, J., Liu, K., Liu, L., Pan, Z.: 2016, On the Magnetic and Energy Characteristics of Recurrent Homologous Jets from An Emerging Flux. *Astrophys. J.* **833**, 150. DOI. ADS.

Liu, Y., Zhao, X., Hoeksema, J.T.: 2004, Correction of Offset in MDI/SOHO Magnetograms. *Solar Physics* **219**, 39. DOI.

López Fuentes, M.C., Démoulin, P., Mandrini, C.H., van Driel-Gesztelyi, L.: 2000, The counterkink rotation of a non-Hale active region. *Astrophys. J.* **544**, 540. DOI.

Luoni, M.L., Démoulin, P., Mandrini, C.H., van Driel-Gesztelyi, L.: 2011, Twisted Flux Tube Emergence Evidenced in Longitudinal Magnetograms: Magnetic Tongues. *Sol. Phys.* **270**, 45. DOI. ADS.

Poisson, M., Démoulin, P., López Fuentes, M., Mandrini, C.H.: 2016, Properties of Magnetic Tongues over a Solar Cycle. *Sol. Phys.* **291**, 1625. DOI. ADS.

Poisson, M., López Fuentes, M.C., Mandrini, C.H., Démoulin, P., MacCormack, C.: 2020a, Correcting the effect of magnetic tongues on the tilt angle of bipolar active regions. *A&A* **633**, A151. DOI. https://doi.org/10.1051/0004-6361/201936924.

Poisson, M., Démoulin, P., Mandrini, C.H., Fuentes, M.C.L.: 2020b, Active-region Tilt Angles from White-light Images and Magnetograms: The Role of Magnetic Tongues. *The Astrophysical Journal* **894**, 131. DOI. https://doi.org/10.3847/1538-4357/ab8944.

Poisson, M., Grings, F., Mandrini, C.H., López Fuentes, M., Démoulin, P.: 2022, Bayesian approach for modeling global magnetic parameters for the solar active region. *A&A* **665**, A101. DOI. https://doi.org/10.1051/0004-6361/202244058.

Poisson, M., López Fuentes, M., Mandrini, C.H., Démoulin, P., Grings, F.: 2024, Modeling Global Magnetic-Flux Emergence in Bipolar Solar-Active Regions. *Sol. Phys.* **299**, 56. DOI. ADS.

Poisson, M., Démoulin, P., López Fuentes, M., Mandrini, C.H.: 2025, Bayesian Modeling of Emerging Bipolar Active Regions from Solar Cycle 23. *Sol. Phys.* **submitted**.

Scherrer, P.H., Bogart, R.S., Bush, R.I., Hoeksema, J.T., Kosovichev, A.G., Schou, J., Rosen-berg, W., Springer, L., Tarbell, T.D., Title, A., Wolfson, C.J., Zayer, I., MDI Engineering Team: 1995, The Solar Oscillations Investigation - Michelson Doppler Imager. *Sol. Phys.* **162**, 129. DOI. ADS.

Schrijver, C.J., Zwaan, C.: 2000, *Solar and Stellar Magnetic Activity.* ADS.

Stenflo, J.O., Kosovichev, A.G.: 2012, Bipolar Magnetic Regions on the Sun: Global Analysis of the SOHO/MDI Data Set. *Astrophys. J.* **745**, 129. DOI. ADS.

Toriumi, S., Wang, H.: 2019, Flare-productive active regions. *Living Reviews in Solar Physics* **16**, 3. DOI. ADS.

Török, T., Downs, C., Linker, J.A., Lionello, R., Titov, V.S., Mikić, Z., Riley, P., Caplan, R.M., Wijaya, J.: 2018, Sun-to-Earth MHD Simulation of the 2000 July 14 "Bastille Day" Eruption. *Astrophys. J.* **856**, 75. DOI. ADS.

Yeates, A.R., Cheung, M.C.M., Jiang, J., Petrovay, K., Wang, Y.-M.: 2023, Surface Flux Transport on the Sun. *Space Sci. Rev.* **219**, 31. DOI. ADS.